Improving the estimation of prognosis for glioblastoma patients by MR based Hemodynamic Tissue Signatures

Elies Fuster-Garcia*[1] | Javier Juan-Albarracín[1] | Germán A García-Ferrando[1] | Luís Martí-Bonmatí[1,1] | Fernando Aparici-Robles[1,1] | Juan M García-Gómez[1]

[1]Instituto Universitario de Tecnologías de la Información y Comunicaciones, Universitat Politècnica de València, València, Spain

[2]Medical Imaging Department, La Fe Polytechnics and University Hospital , València, Spain

[3]Imaging Research Group (GIBI230), La Fe Health Research Institute, València, Spain

Correspondence

*Elies Fuster-Garcia, Universitat Politècnica de València (UPV), Camí de Vera, s/n, 46022, Edifici 8-G, Accés B, planta 1. Email: elfusgar@itaca.upv.es

Present Address

This is sample for present address text this is sample for present address text

Summary

Advanced MR imaging and molecular markers have been raised as crucial to improve prognostic models for patients having glioblastoma lesions. In particular, different MR perfusion based markers describing vascular intrapatient heterogeneity have been correlated with tumor aggressiveness, and represent a key information to understand tumor resistance against effective therapies of these neoplasms. Recently, hemodynamic tissue signature markers based on magnetic resonance perfusion images have been demonstrated useful for describing the heterogeneity of glioblastoma at voxel level, as well as demonstrated significant correlations with patient's overall survival. In this work, we analyze the capabilities of these markers to improve the conventional prognostic models based on clinical, morphological, and demographic features. Our results, both in the regression and classification tests, show that the inclusion of the hemodynamic tissue signature markers improves the reliability of prognostic models. The hemodynamic tissue signature method is fully automatic and it is available for research use at http://www.oncohabitats.upv.es.

KEYWORDS:

glioblastoma, habitats, intrapatient heterogeneity, hemodynamic tissue signatures, perfusion weighted imaging

LIST OF ACRONYMS

AIF Arterial Input Function

CBV Cerebral Blood Volume

CBF Cerebral Blood Flow

CNN Convolutional Neural Networks

DCA-SVFMM Directional Class Adaptive Spatially Varying Finite Mixture Model

DSC Dynamic Susceptibility Contrast

ET Enhancing Tumor

GBM Glioblastoma

HAT High Angiogenic enhancing Tumor

HTS Hemodynamic Tissue Signatures

IPE potentially Infiltrated Peripheral Edema

KPS Karnofsky Performance Status

LAT Low Angiogenic enhancing Tumor

MR Magnetic Resonance

MTT Mean Transit Time

OS Overall Survival

PC Principal Component

PCA Principal Component Analysis

PWI Perfusion Weighted Imaging

CBV Cerebral Blood Volume

CBF Cerebral Blood Flow

rCBV relative Cerebral Blood Volume

rCBF relative Cerebral Blood Flow

rCBV$_{max}$ maximum relative Cerebral Blood Volume

rCBF$_{max}$ maximum relative Cerebral Blood Flow

RMSE Root Mean Squared Error

SNR Signal-to-Noise Ratio

ROI Region of Interest

T1c T1-weighted post gadolinium acquisitions

VPE Vasogenic Peripheral Edema

INTRODUCTION

Glioblastoma (GBM) is the most frequent primary brain tumor[O]. GBM has a poor prognostic with an average survival of 14.6 months for patients undergoing Stupp standard treatment[S]. The main clinical prognostic factors in GBM include patient age, Karnofsky Performance Status (KPS), and the extent of surgical resection[A,F,L,W].

In the last decade, the prognostic models for patients diagnosed with GBM have been significantly improved by adding the molecular profiling to the classical predictors based in clinical and demographic factors[L,M,M]. Even, for the first time, in 2016 the classification of central nervous system tumors of the World Health Organization introduced molecular markers along with histology to describe the interpatient GBM heterogeneity associated with differential prognoses and responses to therapy[B,C,L].

In addition to the interpatient heterogeneity, the GBM is characterized by high intrapatient heterogeneity. This heterogeneity has been identified as one of the factors associated with their high aggressiveness[L], representing a key factor to understand tumor resistance against effective therapies[S]. Traditionally, the in-vivo study of GBM tissue heterogeneity includes three main Region of Interest (ROI)s: enhancing tumor, edema, and necrosis. These ROIs are usually delineated using the information provided by morphological Magnetic Resonance (MR) imaging sequences such as T1-weighted, T2-weighted, FLAIR and T1-weighted post gadolinium acquisitions (T1c). Recent approaches, however, are focusing on the definition of functional habitats based on tissue features at the voxel scale through the information provided by MR imaging sequences such as diffusion weighted imaging, Perfusion Weighted Imaging (PWI), or magnetic resonance spectroscopy, among others[F,D,J,P,C,C].

These complex studies describing the heterogeneity of GBM at voxel level require the use of automated multiparametric image analysis methods [A,C,J,J,Y]. In particular, the study of Juan-Albarracín et al. [J] proposed a methodology to describe GBM vascular intrapatient heterogeneity based on a structured unsupervised multiparametric image analysis technology. This methodology delineates multiparametric habitats so called Hemodynamic Tissue Signatures (HTS) that share similar MR imaging perfusion features within the habitat. A high correlation was found between these HTS perfusion based markers and the Overall Survival (OS) of the patients studied [J]. This correlation might reflect that GBM aggressiveness is associated to a high angiogenic capacity. These results are consistent with the consideration of perfusion markers among the most consistently recognized independent predictors of survival [H,L] and glioma grade progression [C,U,A,C].

In this work, we analyze the usefulness of these markers for improving the estimation of OS in patients with GBM. To this end, first we study the capability of HTS based perfusion markers to improve the multiparametric prognostic models based on standard clinical, morphological, and demographic features. Secondly, we compare the added value of using HTS based markers instead of traditional perfusion parameters (i.e. relative Cerebral Blood Volume (rCBV) and relative Cerebral Blood Flow (rCBF) in Enhancing Tumor (ET) or edema standard ROIs) to improve the estimation of OS. To do so, we performed multiparametric Cox regression analyses in a cross-validation schema to evaluated the results in terms of Root Mean Squared Error (RMSE) and in terms of long vs short survival classification accuracy. Besides, it is important to mention that, in contrast to the study by Abarracín et al. [J], in this study, both morphological segmentation and standardization of perfusion values are performed using fully automatic procedures. This reduces potential biases introduced by the human factor and ensures repeatability and robustness of the results.

MATERIALS

Patient selection

This retrospective study was approved by the institutional reviews of both the hospital and the university. A total of 84 patients with suspected GBM were recovered from 2012 to 2016. The MR images from these patients were also used in the study by Abarracín et al. [J]. The inclusion criteria of the study were: a) GBM with histopathological confirmation; b) complete preoperative MR study including morphological (T1, T2, T1c and FLAIR) and Dynamic Susceptibility Contrast (DSC) MR perfusion series; c) patients undergoing standard Stupp treatment [S], d) partial or total resection, e) KPS > 80; and f) good quality fitting of the DSC perfusion signals to the monocompartimental model in the lesion (gamma-variate R^2 goodness of fit > 0.95). A total of 60 patients met the inclusion criteria, with an overall mean age of 61.1 years and range $[25 - 80]$ years. There were 36 males, with average age of 59.9 years and range $[25 - 80]$, years; and 24 females with average age of 62.9 years and range $[36 - 75]$ years. Mean survival of the population was 402 days.

In this study, we included main clinical, demographic and morphological variables presented in most prognostic studies [A,F,L,W]. These variables comprises: age, gender, resection type, tumor shape, proximity to ventricles, laterality, completeness of the radiochemotherapy (concomitant temozolamide plus total dose of 60Gy radiotherapy), tumor and edema volumes, and tumor location. It is important to notice that the KPS, found relevant in several studies, was not included as prognostic variable as it was used as an inclusion criteria. The variable *completeness of the radiochemotherapy* define the patients that did not receive the concomitant temozolamide plus the 60Gy of radiotherapy defined by the Stupp standard protocol [S]. Finally, GBM molecular profiles based on the IDH1/2 gene status cannot be included in the study because they were not assessed from the post-surgical samples, although they are proven to be related to patient OS.

MR imaging

Standard of care MR exams were obtained from either a 1.5T or 3T Signa HDxt v16 machines (GE Healthcare, Waukesha, WI, USA) with an 8-channel array head coil. From a total of 60 exams included in the study, 48 exams were obtained with 1.5T scanners while the remaining 12 were obtained with 3T scanners. MR sequences included a pre- and post-gadolinium T1-weighted 3D spoiled gradient echo (SPGR) with inversion recovery ($6 - 10/2 - 4$ms TR/TE; 256x256 matrix; 1.5mm slice thickness; 24x24cm FOV; 400ms TI; $70 - 80°$ flip angle), FSE T2-weighted ($3000 - 4000/100 - 110$ms TR/TE; 256x256 matrix; 5mm slice thickness; 21.9x21.9cm FOV; 1 signal acquired; 2mm intersection gap) and FLAIR images ($8000 - 9000/140 - 165$ms TR/TE; 256x192 matrix; 5mm slice thickness; 22x22cm FOV; 1 signal acquired; 2mm intersection gap; 2.200ms TI). The DSC T2*-weighted gradient-echo perfusion study was performed during the injection of a gadolinium-based contrast agent (Multihance, Bracco, Italy). A bolus injection of 0.1 mmol/kg of the contrast agent was administered at 5 ml/s using a power injector (no pre-bolus administration). Saline was injected after the contrast agent (40 ml at the same injection rate). The study was acquired with the following parameters: 2000/25ms TR/TE; 128x128 matrix (1.8x1.8mm in-plane resolution); 7mm slice thickness; 60° flip angle, 14cm full coverage cranio-caudal (20 slices), 40 sequential temporally equidistant volumes each one with an acquisition time of 2 seconds. The baseline before bolus injection was established at 5 dynamics.

METHODS

DSC quantification and HTS analysis

Cerebral Blood Volume (CBV) and Cerebral Blood Flow (CBF) maps were obtained through the standard algorithm proposed by Liu et al.[L]. Only concentration-time curves with Signal-to-Noise Ratio (SNR)> 5 and a goodness of fit $R^2 > 0.95$ to the bivariate gamma function were quantified. Post-processing technique based on the Boxerman et. al[B] leakage correction method was used to correct for over- and under-estimations of CBV and CBF markers. The relatives values maximum relative Cerebral Blood Volume ($rCBV_{max}$) and maximum relative Cerebral Blood Flow ($rCBF_{max}$) were obtained by dividing the values each perfusion marker within the ROI by the median value of the perfusion marker in the contralateral white matter. ROIs were automatically defined for the contralateral white matter areas. To do so, we combine the information of a registered white matter probability mask with the vascular information of CBV maps, to select high probable contralateral white matter regions with lower CBV values. A divide-and-conquer approach was employed to automatically select the Arterial Input Function (AIF). The method performs as follow: perfusion concentration-time signals of the study were recursively divided into two groups by selecting the curves with higher peak height, earliest time to peak and shortest washout, i.e. lowest full width at half maximum. The median of these features was employed to split the groups. Such process was repeated iteratively until 10 or fewer curves were retained. Finally, we compute the AIF as the average of these curves.

Enhancing tumor and edema ROIs delineations were performed using Convolutional Neural Networks (CNN) algorithm. This algorithm uses the information of post-gadolinium T1-weighted, T2-weigted, and FLAIR sequences, and it is based on a U-net architecture[R] with a contracting and expanding paths of 4 residual-blocks preceded of 4 simple-blocks. All convolutions use isotropic kernels of 3x3x3. The CNN was trained on the BRATS 2017 challenge dataset[M], using Adam Optimizer and cross-entropy as loss function. L2 regularization was employed to avoid for overtting during training process.

Once the enhancing tumor and edema ROIs were delineated we computed the HTS. HTS consists of a set of vascular habitats detected in GBM, which were defined by Javier et al. in [J]. The method to obtain the HTS is based on Directional Class Adaptive Spatially Varying Finite Mixture Model (DCA-SVFMM)[J,J], which consists of a clustering algorithm that combines Gaussian mixture modeling with continuous Markov Random Fields. The HTS defines four habitats within GBM with similar vascular properties: the High Angiogenic enhancing Tumor (HAT) and Low Angiogenic enhancing Tumor (LAT) habitats, and the potentially Infiltrated Peripheral Edema (IPE) and the Vasogenic Peripheral Edema (VPE) habitats. The HTS habitats used in this study were obtained following the original fully automatic and unsupervised algorithm proposed by Albarracín et al.[J], which results in the application of the DCA-SVFMM method inside the ROI of the tumor lesion. The method is available for non-clinical use at http://www.oncohabitats.upv.es as a free online service. Once registered, users can upload their images and receive the results via e-mail. The online service does not only offer the use of the methodology free of charge, but it also provides the computer infrastructure for the analysis. The results provided by the oncohabitats service include: the processed uploaded images, the perfusion parametric maps (rCBV, rCBF, Mean Transit Time (MTT), K2) , the GBM segmentation mask, the HTS mask with the habitat's delineation, and a summary report in pdf format.

The DSC-PWI based variables included in the study comprise the maximum values of relative CBV, and relative CBV at the two main ROIs in GBM (i.e. $rCBV_{max}$ and $rCBF_{max}$ at enhancing tumor and edema), and at the four habitats defined within GBM (i.e. $rCBV_{max}$ and $rCBF_{max}$ at HAT, LAT, IPE, and VPE). To obtain a robust estimation of the maximum values at each habitat for each perfusion marker we consider not the maximum value but the value of the 90 percentile. In Figure an example of the HTS results obtained for three different patients is presented.

Selection of input variables

In order to select the most informative variables to build the prognostic models, categorical discrete variables and numerical continuous variables were differentiated. Kaplan-Meier log-rank analysis was performed for categorical variables. The obtained p-value determine the statistical relationship of the categorical variables in the survival functions. In addition, the Mantel-Haneszel Hazard Ratio value shows the influence of the variable in the patient OS. Cox proportional hazard regression and Wald significance test were conducted for numerical continuous variables. Hazard ratios, confidence intervals at 95% and p-values were calculated. Once the uniparametric analyses were performed, those variables with significant ($p< 0.05$) were selected to build the prognostic multiparametric models.

Before generating the multiparametric models, we decorrelated the HTS variables found significant in the uniparametric analysis by performing a Principal Component Analysis (PCA). Only the first Principal Component (PC) was retained; we will refer to as HTS 1st PC. Analogously, we decorrelated the ET perfusion variables using PCA, and retained the first PC, so called ET 1st PC.

Finally, in order to analyze the influence of the HTS 1st PC on a multiparametric regression model, a multivariate Cox regression analysis was performed including those variables yielding statistically significant correlation with OS in the uniparametric analysis. This analysis will assess whether the new predictor (i.e. HTS 1st PC) is statistically significant in a multivariable model including all significant clinical, morphological, and demographic variables.

Multiparametric prognostic models

To assess the added value of HTS 1st PC for the improvement of GBM prognostic models, we generated three different multiparametric prognostic models: Model 1) using only the clinical and demographic variables, Model 2) adding to Model 1 the information of the ET 1st PC and Model 3) adding to model 1 the information of the HTS 1st PC. We compared the differences between the predicted and real OS obtained by the different multivariate Cox regression based models.

Additionally, we evaluated the capability to stratify patients between large and short survivors of all multivariate Cox regression models. The patients have been tagged as large survivors if their predicted OS was greater than the mean OS of the study population (402 days), and tagged as short survival if their predicted OS was greater than the mean OS of the population. These stratification capabilities were evaluated by means of a Kaplan-Meier test, and the computation of the prediction accuracy.

Evaluation and figures of merit

We used the RMSE metric to evaluate the differences between the predicted and real OS obtained by the multivariate Cox regression based models. The RMSE is defined as $\text{RMSE} = \sqrt{\frac{1}{n}\sum_{i=1}^{n}(\widehat{OS_i} - OS_i)^2}$, where n is the total number of samples, OS_i is the overall survival of patient i, and $\widehat{OS_i}$ is the predicted overall survival of patient i. To test if differences in RMSE were statistically significant, a paired Wilcoxon signed rank test single tailed was conducted.

Complementarily, to asses the capability of the multivariate Cox regression models to stratify patients between large and short survivors, we used the accuracy metric. That is, the number correctly classified samples divided by the total number of samples.

The figures of merit based on RMSE and stratification accuracy have been computed using only non-censored cases with exitus date registered (i.e. 50 cases).The software used to perform the statistical tests, prognostic models, and evaluations was MATLAB® 2017a.

RESULTS

Selection of input variables

The results of the Kaplan-Meier log-rank analysis for the categorical discrete variables are summarized in Table 1. The test revealed that several variables were able to generate populations with significant OS differences ($p < 0.05$). These significant variables were: biopsy instead of total or partial resection, a large or small distance to ventricles, frontal tumor location, and complete or incomplete radiochemotherapy.

The results of the survival study based on the uniparametric Cox proportional hazards model for the continuous variables are presented in Table 2. Based on these results, the variables found significant ($p < 0.05$) were: $rCBF_{max}$ at enhancing tumor, HAT, LAT and IPE, $rCBV_{max}$ at enhancing tumor, HAT, LAT and IPE, enhancing tumor volume, and patient's age.

The values of rCBV and rCBF are quite correlated in the HAT, LAT, and IPE habitats ($r = 0.83$, $r = 0.70$, $r = 0.93$ respectively). Analogously, perfusion values in the two habitats corresponding to the ET (i.e. HAT and LAT) also show an important correlation ($r = 0.83$ in rCBV and $r = 0.71$ in rCBF). On the contrary, there is a much lower correlation between the perfusion values HAT habitat and the IPE habitat located in the peritumoral region ($r = 0.37$ for rCBV and $r = 0.46$ for rCBF). Finally, only a moderate correlation can be seen between perfusion values in LAT and IPE of $r = 0.60$ for rCBV and $r = 0.68$ for rCBF.

We performed PCA on the HTS variables found significant in the uniparametric analysis to avoid correlated variables. The HTS 1st PC describes the 69.13% of the significant HTS variables variance. It is defined mathematically as follows (Eq. 1):

$$\text{HTS}1st\text{PC} = \begin{pmatrix} 0.1171 & 0.2973 & 0.7501 & 0.1025 & 0.4285 & 1.0793 \end{pmatrix} * \begin{pmatrix} rCBV_{HATmax} \\ rCBV_{LATmax} \\ rCBV_{IPEmax} \\ rCBF_{HATmax} \\ rCBF_{LATmax} \\ rCBF_{IPEmax} \end{pmatrix} + 8.5763 \tag{1}$$

Analogously, we decorrelated the ET perfusion variables using PCA, and retained the first PC. From the classical ROIs, edema and ET, only the ET was found significant in the uniparametric analysis. The ET 1st PC describes the 94, 1% of the significant perfusion variables variance. It is defined mathematically as follows (Eq. 2):

$$\text{ET}1st\text{PC} = \begin{pmatrix} 0.2601 & 0.2443 \end{pmatrix} * \begin{pmatrix} rCBV_{ETmax} \\ rCBF_{ETmax} \end{pmatrix} - 3.7326 \tag{2}$$

The variables found significant ($p < 0.05$) in the multiparametric model were: patient age, distance of the tumor to ventricles, radiochemotherapy, and HTS 1st PC. In particular, the HTS 1st PC value obtained the lowest p-value of all the variables included in the multivariate Cox regression analysis of prognostic factors. These results are presented in Table 3.

Multiparametric prognostic models

We tested the prognostic capabilities of the three different multiparametric models defined in Methods section. The results obtained through a train-test scheme based on a leave-one-out strategy shows that the Model 1 (based on clinical and demographic information) obtained an RMSE = 219.33 days, the Model 2 (based on inputs of Model 1 + ET 1st PC) obtained an RMSE = 202.39 days, and finally the Model 3 (based on inputs of Model 1 + HTS 1st PC) obtained an RMSE = 183.57 days. This means that, while Model 2 improves the prognostic estimation of Model 1 in a 7.7%, Model 3 outperforms this improvement up to the 16.3% in terms of RMSE. These differences between RMSE were significant between Model 1 and Model 3 based on a Wilcoxon signed rank paired test ($p < 0.05$). However, these differences have not found significant between Model 1 and Model 2. The performance results of the models are presented in Figure . The data presented in the figure correspond to the predictions generated for each of the test patient in each iteration of the leave-one-out cross-validation evaluation.

Finally, we compared the ability of all three models to stratify the population between long and short survivors. The results obtained using the multiparametric models have been summarized in the Kaplan-Meier curves presented in Figure . The stratification generated by the Model 3 (on the right) obtained an accuracy=78.0%. This outperforms the stratification capabilities of the Model 1 (on the left), and of the Model 2 that includes information of HTS 1st PC (on the middle), that obtained an accuracy=74.0% and an accuracy=76.0% respectively.

DISCUSSION

One of the most interesting results is the positive correlation of the hemodynamic indices at the IPE habitat to predict patient's survival (p<0.05 for $rCBV_{max}$ and $rCBV_{max}$ at IPE region, see Table 2). The association between peritumoral areas and OS does not appear when analyzing the gross region of the edema (p>0.05 for $rCBV_{max}$ and $rCBV_{max}$ at edema region see Table 2). According to the study of Lemee[L], this region is of a particular interest due the high rate of local recurrence in the peritumoral brain zone. Although, DSC k_{trans} has been proven as the most sensitive and specific predictor of brain infiltration and histological grading[Z], recent studies also showed that DCE MR imaging parameters in specific areas of GBM related to the IPE are correlated with biomarkers of hypoxia and overall patient survival[J,A,J,J]. These evidences support the results obtained on the importance of IPE habitat to the improvement of GBM patients prognostic estimation.

When we analyze the results of the three different multiparametric Cox regression models, those that include MRI data do better than those that are only considered clinical data. This result provides us with evidence of the complementary information that DSC perfusion markers can provide for GBM management. Additionally, what is particularly interesting in the results obtained is that, while the inclusion of the ET 1st PC improves the GBM prognostic estimation in a 7.7% in terms of the RMSE, the HTS 1st PC outperforms this improvement up to the 16.3%. Only the improvement obtained by the inclusion of the HTS 1st PC have been proven statistically significant. Perfusion measures in HAT and LAT were shown poorly correlated with those in IPE. This could mean that perfusion measures in ET related habitats (i.e. HAT and LAT) habitats may provide different information compared with those in infiltrative tumor region (i.e. IPE). This complementary information included in the HTS 1st PC may be at the basis of the improvement in OS prediction. These results reinforce the evidence for the need for a better characterization of the heterogeneity of GBM in order to improve the current management of the disease. In this sense, we consider that the combination of the molecular profile together with the information obtained through DSC-MR imaging can contribute substantially to the selection of the most suitable therapeutic alternatives for each patient.

The results presented in this study are particularly relevant because the DSC markers as well as ROIs volumes have been obtained automatically without expert interaction. Additionally, the method used in the study is available as a free web service for research. These both factors constitute an important step towards the creation of repeatable studies that allow the application of its conclusions directly to cases collected in the usual clinical practice.

One of the limitations of the study is the absence of the molecular profiling because this was not obtained from patients at the time of diagnosis and subsequent treatment. Although the molecular profile is being demonstrated to be of interest for the management of therapeutic decisions on GBM patients, studies such as the Jain et al.[J] suggests that the hemodynamic imaging biomarkers provide important prognostic information independent of the molecular subclasses. Based on that we consider that, although the inclusion of the molecular profile could affect the prognostic capacity of the models, it would probably affect all prognostic models presented in the study in the same way, and, consequently, it would not change the main conclusions of the study. Another limitation is the fact that the dataset was obtained from a single center. This fact may generate a possible bias in the results due to the influence of procedural factors characteristic of the centre or of the acquisition protocols. Based on these two

limitations, future work should focus on providing novel evidences on the added value of the information provided by HTS to the GBM molecular subtypes classification models, and on replicating this experiment on a multicentric and international dataset. Finally, perfusion studies included in the study have been obtained using the clinical routine protocol established at the hospital. This implies short sequences without preload bolus injection and a low number of dynamics to reduce the acquisition time. Although this could have an effect on the quality of perfusion markers, this risk has been minimized by using concentration curve quality control mechanisms, and by including Boxerman et. al [B] method to correct for over- and under-estimations of rCBV and rCBF markers.

In summary, we have found that the inclusion of the HTS markers improves the reliability of prognostic models, both in the regression and classification tests. The described method is available for research use at http://www.oncohabitats.upv.es.

ACKNOWLEDGMENTS

References

A. Akman, F., Cooper, R. A., Sen, M., Tanriver, Y., and Kentli, S. (2002). Validation of the Medical Research Council and a newly developed prognostic index in patients with malignant glioma: how useful are prognostic indices in routine clinical practice? Journal of Neuro-Oncology, 59(1):39–47.

A. Aronen, H. J., Gazit, I. E., Louis, D. N., Buchbinder, B. R., Pardo, F. S., Weisskoff, R. M., Harsh, G. R., Cosgrove, G. R., Halpern, E. F., and Hochberg, F. H. (1994). Cerebral blood volume maps of gliomas: comparison with tumor grade and histologic findings. Radiology, 191(1):41–51.

A. Artzi, M., Bokstein, F., Blumenthal, D. T., Aizenstein, O., Liberman, G., Corn, B. W., and Ben Bashat, D. (2014). Differentiation between vasogenic-edema versus tumor-infiltrative area in patients with glioblastoma during bevacizumab therapy: a longitudinal MRI study. European Journal of Radiology, 83(7):1250–1256.

B. Bai, H., HarmancÄś, A. S., Erson-Omay, E. Z., Li, J., Coşkun, S., Simon, M., Krischek, B., Özduman, K., Omay, S. B., Sorensen, E. A., Turcan, Ş., BakÄśrcÄśğlu, M., Carrión-Grant, G., Murray, P. B., Clark, V. E., Ercan-Sencicek, A. G., Knight, J., Sencar, L., AltÄśnok, S., Kaulen, L. D., Gülez, B., Timmer, M., Schramm, J., Mishra-Gorur, K., Henegariu, O., Moliterno, J., Louvi, A., Chan, T. A., Tannheimer, S. L., Pamir, M. N., Vortmeyer, A. O., Bilguvar, K., Yasuno, K., and Günel, M. (2016). Integrated genomic characterization of IDH1-mutant glioma malignant progression. Nature Genetics, 48(1):59.

B. Boxerman J.L., Schmainda K.M., W. R. (2006). Relative cerebral blood volume maps corrected for contrast agent extravasation significantly correlate with glioma tumor grade, whereas uncorrected maps do not. AJNR Am J Neuroradiol., 27(4):859–67.

C. Chang, Y.-C. C., Ackerstaff, E., Tschudi, Y., Jimenez, B., Foltz, W., Fisher, C., Lilge, L., Cho, H., Carlin, S., Gillies, R. J., Balagurunathan, Y., Yechieli, R. L., Subhawong, T., Turkbey, B., Pollack, A., and Stoyanova, R. (2017). Delineation of Tumor Habitats based on Dynamic Contrast Enhanced MRI. Scientific Reports, 7(1):9746.

C. Chen, J.-R., Yao, Y., Xu, H.-Z., and Qin, Z.-Y. (2016). Isocitrate Dehydrogenase (IDH)1/2 Mutations as Prognostic Markers in Patients With Glioblastomas. Medicine, 95(9).

C. Choi, Y. S., Kim, D. W., Lee, S.-K., Chang, J. H., Kang, S.-G., Kim, E. H., Kim, S. H., Rim, T. H., and Ahn, S. S. (2015). The Added Prognostic Value of Preoperative Dynamic Contrast-Enhanced MRI Histogram Analysis in Patients with Glioblastoma: Analysis of Overall and Progression-Free Survival. AJNR. American journal of neuroradiology, 36(12):2235–2241.

C. Cui, Y., Tha, K. K., Terasaka, S., Yamaguchi, S., Wang, J., Kudo, K., Xing, L., Shirato, H., and Li, R. (2015). Prognostic Imaging Biomarkers in Glioblastoma: Development and Independent Validation on the Basis of Multiregion and Quantitative Analysis of MR Images. Radiology, 278(2):546–553.

C. Cui, Y., Tha, K. K., Terasaka, S., Yamaguchi, S., Wang, J., Kudo, K., Xing, L., Shirato, H., and Li, R. (2016). Prognostic Imaging Biomarkers in Glioblastoma: Development and Independent Validation on the Basis of Multiregion and Quantitative Analysis of MR Images. Radiology, 278(2):546–553.

D.   Demerath, T., Simon-Gabriel, C. P., Kellner, E., Schwarzwald, R., Lange, T., Heiland, D. H., Reinacher, P., Staszewski, O., Mast, H., Kiselev, V. G., Egger, K., Urbach, H., Weyerbrock, A., and Mader, I. (2017). Mesoscopic imaging of glioblastomas: Are diffusion, perfusion and spectroscopic measures influenced by the radiogenetic phenotype? The Neuroradiology Journal, 30(1):36–47.

F.   Field, K. M., Drummond, K. J., Yilmaz, M., Tacey, M., Compston, D., Gibbs, P., and Rosenthal, M. A. (2013). Clinical trial participation and outcome for patients with glioblastoma: multivariate analysis from a comprehensive dataset. Journal of Clinical Neuroscience: Official Journal of the Neurosurgical Society of Australasia, 20(6):783–789.

F.   Fuster-Garcia, E., García-Gómez, J., De Angelis, E., Sraum, A., Molnar, A., Van Huffel, S., and Stamatakos, G. (2016). Imaging Biomarkers: Development and Clinical Integration. In Use case II: Imaging biomarkers and new trends for integrated glioblastoma management, pages 181–194. Springer International Publishing.

H.   Hirai, T., Murakami, R., Nakamura, H., Kitajima, M., Fukuoka, H., Sasao, A., Akter, M., Hayashida, Y., Toya, R., Oya, N., Awai, K., Iyama, K., Kuratsu, J.-i., and Yamashita, Y. (2008). Prognostic value of perfusion MR imaging of high-grade astrocytomas: long-term follow-up study. AJNR. American journal of neuroradiology, 29(8):1505–1510.

J.   Jain, R., Poisson, L., Narang, J., Gutman, D., Scarpace, L., Hwang, S. N., Holder, C., Wintermark, M., Colen, R. R., Kirby, J., Freymann, J., Brat, D. J., Jaffe, C., and Mikkelsen, T. (2013). Genomic mapping and survival prediction in glioblastoma: molecular subclassification strengthened by hemodynamic imaging biomarkers. Radiology, 267(1):212–220.

J.   Jalali, S., Chung, C., Foltz, W., Burrell, K., Singh, S., Hill, R., and Zadeh, G. (2014). MRI biomarkers identify the differential response of glioblastoma multiforme to anti-angiogenic therapy. Neuro-Oncology, 16(6):868–879.

J.   Jena, A., Taneja, S., Gambhir, A., Mishra, A. K., DÊijsouza, M. M., Verma, S. M., Hazari, P. P., Negi, P., Jhadav, G. K. R., and Sogani, S. K. (2016). Glioma Recurrence Versus Radiation Necrosis: Single-Session Multiparametric Approach Using Simultaneous O-(2-18f-Fluoroethyl)-L-Tyrosine PET/MRI. Clinical Nuclear Medicine, 41(5):e228–236.

J.   Jensen, R. L., Mumert, M. L., Gillespie, D. L., Kinney, A. Y., Schabel, M. C., and Salzman, K. L. (2014). Preoperative dynamic contrast-enhanced MRI correlates with molecular markers of hypoxia and vascularity in specific areas of intratumoral microenvironment and is predictive of patient outcome. Neuro-Oncology, 16(2):280–291.

J.   Juan-Albarracín, J., Fuster-Garcia, E., and García-Gómez, J. (2016). An online platform for the automatic reporting of multi-parametric tissue signatures: A case study in Glioblastoma. Lecture Notes in Computer Science (including subseries Lecture Notes in Artificial Intelligence and Lecture Notes in Bioinformatics), 10154 LNCS:43–51.

J.   Juan-Albarracín, J., Fuster-Garcia, E., Manjón, J., Robles, M., Aparici, F., Martí-Bonmatí, L., and García-Gómez, J. (2015). Automated glioblastoma segmentation based on a multiparametric structured unsupervised classification. PLoS ONE, 10(5).

J.   Juan-Albarracín, J., Fuster Garcia, E., Pérez-Girbes, A., Aparixi-Robles, F, Alberich-Bayarri, A, Revert-Ventura, A., Martí-bonmatí, L, and García-Gómez, JM (2018). Glioblastoma: Vascular Habitats Detected at Preoperative Dynamic Susceptibility-Weighted Contrast-Enhanced Perfusion MR Imaging Predict Survival. Radiology, [Epub ahead of print].

L.   Law, M., Young, R. J., Babb, J. S., Peccerelli, N., Chheang, S., Gruber, M. L., Miller, D. C., Golfinos, J. G., Zagzag, D., and Johnson, G. (2008). Gliomas: predicting time to progression or survival with cerebral blood volume measurements at dynamic susceptibility-weighted contrast-enhanced perfusion MR imaging. Radiology, 247(2):490–498.

L.   Le Mercier, M., Hastir, D., Moles Lopez, X., De Nève, N., Maris, C., Trepant, A.-L., Rorive, S., Decaestecker, C., and Salmon, I. (2012). A simplified approach for the molecular classification of glioblastomas. PloS One, 7(9):e45475.

L.   Lemée, J.-M., Clavreul, A., and Menei, P. (2015a). Intratumoral heterogeneity in glioblastoma: don't forget the peritumoral brain zone. Neuro-Oncology, 17(10):1322–1332.

L.   Lemée, J.-M., Clavreul, A., and Menei, P. (2015b). Intratumoral heterogeneity in glioblastoma: don't forget the peritumoral brain zone. Neuro-Oncology, 17(10):1322–1332.

L.   Liu, T. T., Achrol, A. S., Mitchell, L. A., Rodriguez, S. A., Feroze, A., Iv, M., Kim, C., Chaudhary, N., Gevaert, O., Stuart, J. M., Harsh, G. R., Chang, S. D., and Rubin, D. L. (2017). Magnetic resonance perfusion image features uncover an angiogenic subgroup of glioblastoma patients with poor survival and better response to antiangiogenic treatment. Neuro-Oncology, 19(7):997–1007.

L. Louis, D. N., Perry, A., Reifenberger, G., von Deimling, A., Figarella-Branger, D., Cavenee, W. K., Ohgaki, H., Wiestler, O. D., Kleihues, P., and Ellison, D. W. (2016). The 2016 World Health Organization Classification of Tumors of the Central Nervous System: a summary. <u>Acta Neuropathologica</u>, 131(6):803–820.

L. Lutterbach, J., Sauerbrei, W., and Guttenberger, R. (2003). Multivariate analysis of prognostic factors in patients with glioblastoma. <u>Strahlentherapie Und Onkologie: Organ Der Deutschen Rontgengesellschaft ... [et Al]</u>, 179(1):8–15.

M. Marziali, G., Buccarelli, M., Giuliani, A., Ilari, R., Grande, S., Palma, A., D'Alessandris, Q. G., Martini, M., Biffoni, M., Pallini, R., and Ricci-Vitiani, L. (2017). A three-microRNA signature identifies two subtypes of glioblastoma patients with different clinical outcomes. <u>Molecular Oncology</u>, 11(9):1115–1129.

M. Marziali, G., Signore, M., Buccarelli, M., Grande, S., Palma, A., Biffoni, M., Rosi, A., D'Alessandris, Q. G., Martini, M., Larocca, L. M., Maria, R. D., Pallini, R., and Ricci-Vitiani, L. (2016). Metabolic/Proteomic Signature Defines Two Glioblastoma Subtypes With Different Clinical Outcome. <u>Scientific Reports</u>, 6:21557.

M. Menze, B., Reyes, M., and Van Leemput, K. (2014). The Multimodal Brain TumorImage Segmentation Benchmark (BRATS). <u>IEEE transactions on medical imaging</u>.

O. Ostrom, Q. T., Gittleman, H., Liao, P., Vecchione-Koval, T., Wolinsky, Y., Kruchko, C., and Barnholtz-Sloan, J. S. (2017). CBTRUS Statistical Report: Primary brain and other central nervous system tumors diagnosed in the United States in 2010-2014. <u>Neuro-Oncology</u>, 19(suppl_5):v1–v88.

P. Price, S. J., Young, A. M. H., Scotton, W. J., Ching, J., Mohsen, L. A., Boonzaier, N. R., Lupson, V. C., Griffiths, J. R., McLean, M. A., and Larkin, T. J. (2016). Multimodal MRI can identify perfusion and metabolic changes in the invasive margin of glioblastomas. <u>Journal of magnetic resonance imaging: JMRI</u>, 43(2):487–494.

R. Ronneberger, O., Fischer, P., and Brox, T. (2015). U-Net: Convolutional Networks for Biomedical Image Segmentation. <u>arXiv:1505.04597 [cs]</u>. arXiv: 1505.04597.

S. Soeda, A., Hara, A., Kunisada, T., Yoshimura, S.-i., Iwama, T., and Park, D. M. (2015). The evidence of glioblastoma heterogeneity. <u>Scientific Reports</u>, 5:7979.

S. Stupp, R., Mason, W. P., van den Bent, M. J., Weller, M., Fisher, B., Taphoorn, M. J. B., Belanger, K., Brandes, A. A., Marosi, C., Bogdahn, U., Curschmann, J., Janzer, R. C., Ludwin, S. K., Gorlia, T., Allgeier, A., Lacombe, D., Cairncross, J. G., Eisenhauer, E., Mirimanoff, R. O., European Organisation for Research and Treatment of Cancer Brain Tumor and Radiotherapy Groups, and National Cancer Institute of Canada Clinical Trials Group (2005). Radiotherapy plus concomitant and adjuvant temozolomide for glioblastoma. <u>The New England Journal of Medicine</u>, 352(10):987–996.

U. Ulyte, A., Katsaros, V. K., Liouta, E., Stranjalis, G., Boskos, C., Papanikolaou, N., Usinskiene, J., and Bisdas, S. (2016). Prognostic value of preoperative dynamic contrast-enhanced MRI perfusion parameters for high-grade glioma patients. <u>Neuroradiology</u>, 58(12):1197–1208.

W. Wang, K., Wang, Y., Fan, X., Wang, J., Li, G., Ma, J., Ma, J., Jiang, T., and Dai, J. (2016). Radiological features combined with IDH1 status for predicting the survival outcome of glioblastoma patients. <u>Neuro-Oncology</u>, 18(4):589–597.

Y. You, D., Kim, M. M., Aryal, M. P., Parmar, H., Piert, M., Lawrence, T. S., and Cao, Y. (2018). Tumor image signatures and habitats: a processing pipeline of multimodality metabolic and physiological images. <u>Journal of Medical Imaging (Bellingham, Wash.)</u>, 5(1):011009.

Z. Zhang, N., Zhang, L., Qiu, B., Meng, L., Wang, X., and Hou, B. L. (2012). Correlation of volume transfer coefficient Ktrans with histopathologic grades of gliomas. <u>Journal of magnetic resonance imaging: JMRI</u>, 36(2):355–363.
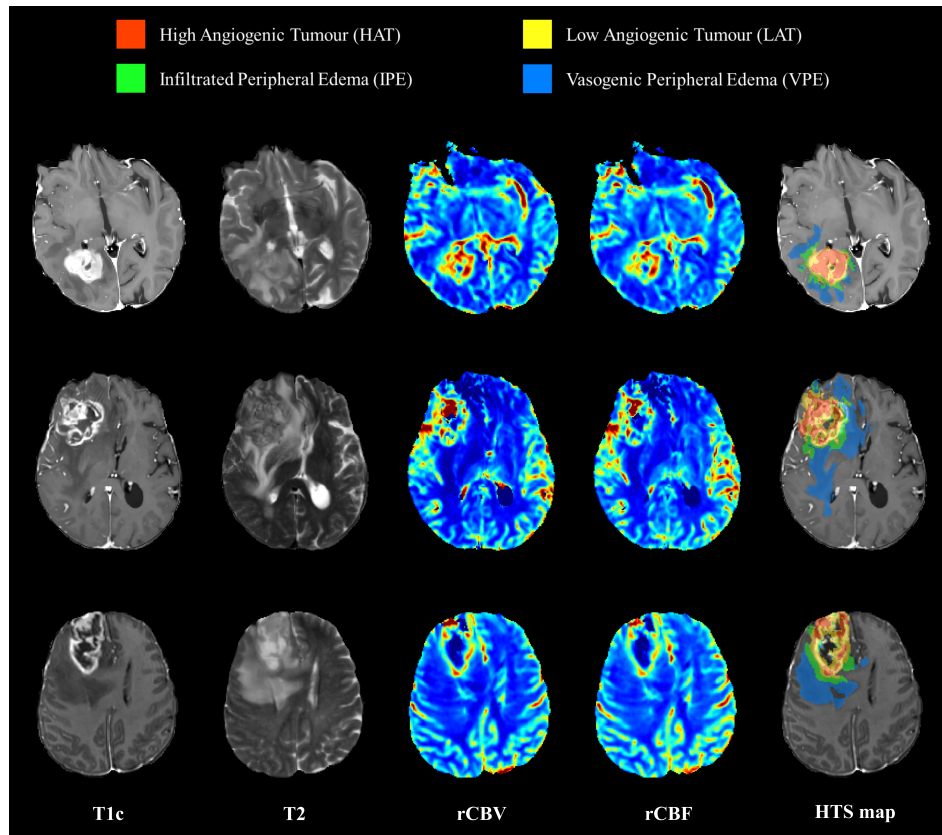
FIGURE 1 Example of three HTS maps. For each case, from left to right: post-GBCA T1-weighted MR imaging, T2-weighted MR imaging, cerebral blood volume (CBV) map, cerebral blood flow (CBF) map and HTS habitats map over the post-gadolinium-based contrast agent T1-weighted MR imaging.
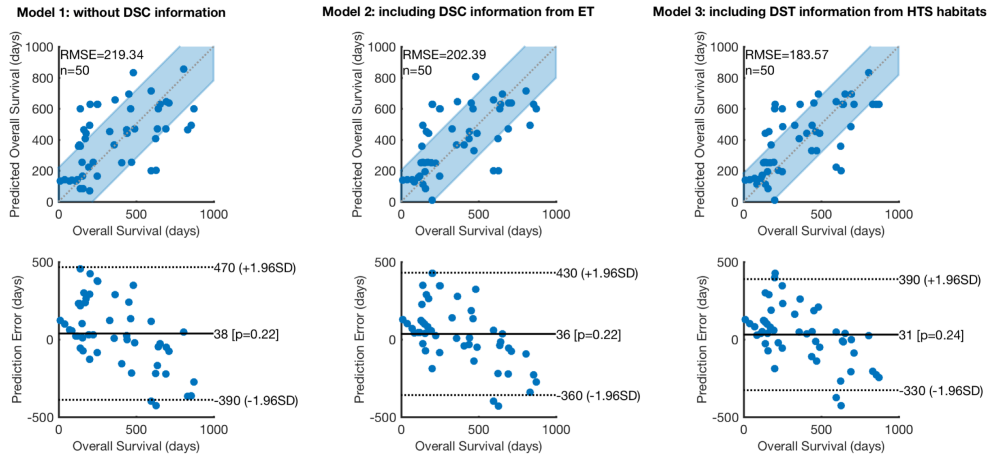
FIGURE 2 Scatter plot for predicted vs real overall survival (top) and Bland-Altman plot (bottom) for different multiparametric regression models: Model 1) without DSC information (on the left), Mode 2) including DSC information at ET (on the middle), and Model 3) including DSC information at HAT, LAT, and IPE ROIs defined by the HTS (on the right). The red line represents the area where the points should fall in the case of an ideal hypothetical regression.
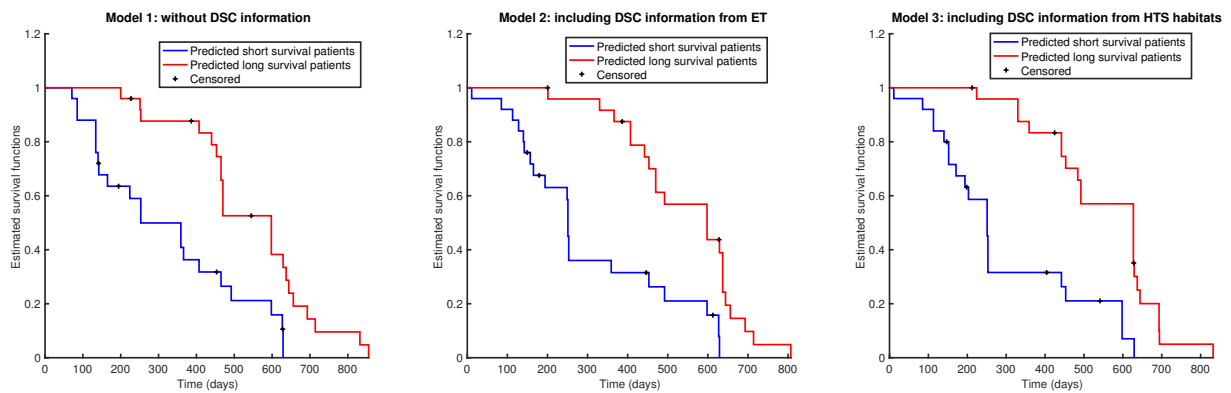
FIGURE 3 Kaplan-Meier curves comparing the capability of the three multiparametric models to stratify the population between long and short survivors: Model 1) multiparametric model without DSC information (on the left), Model 2) multiparametric model including DSC information at ET (on the middle), and Model 3) multiparametric model including DSC information at HAT, LAT, and IPE ROIs defined by the HTS (on the right).

TABLE 1 Results of the uniparametric Kaplan-Meier test on the categorical discrete variables included in the study. * Indicates a significant difference (p<0.05).

	Population	Mean Survivals	p-value
Gender	[36 24]	[437, 349]	0.522
Laterality	[24 33]	[487, 371]	0.525
Resection			
- Total	[20 40]	[562, 322]	0.025*
- Subtotal	[34 26]	[356, 462]	0.262
- Biopsy (no resection)	[6 54]	[129, 432]	0.001*
Distance to ventricles			
- Large	[20 40]	[575, 316]	0.002*
- Mid	[21 39]	[391, 408]	0.957
- Small	[19 41]	[233, 481]	310^{-5}*
Location			
- Frontal	[14 46]	[299, 433]	0.028*
- Parietal	[14 46]	[465, 383]	0.217
- Temporal	[27 33]	[391, 411]	0.962
- Occipital	[5 55]	[573, 386]	0.525
Radiochemotherapy			
- Complete	[49 11]	[465, 122]	310^{-11}
- Incomplete	[5 55]	[173, 423]	0.006*

TABLE 2 Results of the uniparametric Cox proportional hazards model on the numerical continuous variables included in the study. * Indicates a significant difference (p<0.05).

	HR [exp(bi)]	95% CI	p-value
Cerebral Blood Volume			
- *Enhancing Tumor*	1.23	[1.10-1.37]	$4 10^{-4}$ *
- *Edema*	1.20	[0.94-1.54]	0.134
- *HAT*	1.14	[1.06-1.23]	$6 10^{-4}$*
- *LAT*	1.28	[1.07-1.52]	0.007*
- *IPE*	1.89	[1.07-3.34]	0.027*
- *VPE*	1.84	[0.99-3.42]	0.052
Cerebral Blood Flow			
- *Enhancing Tumor*	1.24	[1.11-1.37]	$8 10^{-5}$*
- *Edema*	1.28	[0.93-1.75]	0.12686
- *HAT*	1.16	[1.08-1.39]	$4 10^{-5}$*
- *LAT*	1.44	[1.07-1.93]	0.015*
- *IPE*	2.57	[1.12-5.91]	0.027*
- *VPE*	2.31	[0.95-5.64]	0.065
Volumes			
- *Enhancing Tumor*	1.02	[1.00-1.03]	0.012*
- *Edema*	1.00	[0.99-1.01]	0.979
- *HAT*	1.06	[1.01-1.11]	0.011*
- *LAT*	1.03	[1.01-1.06]	0.006*
- *IPE*	1.01	[0.98-1.05]	0.401
- *VPE*	1.00	[0.99-1.01]	0.917
Age	1.08	[1.01-1.07]	0.007*

TABLE 3 Multiparametric Cox proportional hazards model built on the variables found in the study uniparametrically statistically significant. * Indicates a significant difference (p<0.05).

	HR [exp(bi)]	95% CI	p-value
Age	1.03	[1.004-1.060]	0.026*
Distance to ventricles	0.52	[0.300-0.910]	0.022*
Resection	2.35	[0.734-7.556]	0.150
Location	1.60	[0.730-3.512]	0.240
Enhancing Tumor Volume	0.99	[0.969-1.014]	0.439
Radiochemotherapy	0.28	[0.093-0.831]	0.022*
HTS 1st Princ. Comp.	1.21	[1.013-1.451]	0.035*